Temporally Aliased Video Microscopy: An Undersampling Method for In-Plane Modal Analysis of Microelectromechanical Systems

Christophe Yamahata, Marc Stranczl, Edin Sarajlic, Gijs J. M. Krijnen, *Member, IEEE*, and Martin A. M. Gijs

***Abstract*—A simple optical method is proposed for performing in-plane experimental modal analysis of micromachined structures with a conventional charge-coupled device (CCD) camera. The motion of a micromechanical device actuated by high-frequency sinusoidal forces (kilohertz range) is recorded at the fixed sampling rate of a camera (typically, 28 frames/s) which is configured with a short shutter aperture time (1/5000 s). Provided a CCD sensor with sufficient sensitivity, much information is contained in the video on the dynamics of the vibrating system despite the limited frame rate. Taking advantage of the theory of undersampling, we show that the dynamics of the systems with several-kilohertz bandwidth can be retrieved very easily. For demonstration purposes, we first study a push–pull electrostatic comb-drive actuator, which is a well-known damped harmonic oscillator system. Then, we show that our measurement method also provides useful information on the behavior of nonlinear systems. In particular, we can characterize the systems' superharmonic and subharmonic resonances in a straightforward way. [2011-0281]**

***Index Terms*—Folding frequency, image analysis, in-plane vibration, microelectromechanical systems (MEMS) characterization, modal analysis, Nyquist criterion, optical measurement, resonant frequency, subharmonic, superharmonic, undersampling, video microscopy.**

I. Introduction

MICROMACHINED devices usually have a functionality that is directly dependent on their static and dynamic mechanical properties. On the other hand, downscaling is inevitably accompanied with an increasing dependence of physical characteristics to material imperfections and to variability in manufacturing. This raises the question of how to reconcile miniaturization with the finiteness of process capabilities. Let us consider, for instance, the cantilever in an atomic force microscope (AFM). Experiments performed with an AFM are based on measuring the deflection of a thin cantilever whose spring constant must, in turn, be known with ultimate accuracy. However, the mechanical stiffness of thin films is most sensitive to the variation of thickness, which is also a parameter that is difficult to control in fabrication. Nevertheless, the spring constant of a cantilever can be indirectly estimated from its frequency response function. The "thermal tune method" is a well-established calibration method that is routinely used for that purpose. It consists in measuring the cantilever's out-of-plane dynamic response to thermal noise [1]. This example is an illustration that manufacturing of microelectromechanical systems (MEMS) not only requires perfect control of fabrication technologies but also involves systematic testing of the microfabricated devices, including their dynamic mechanical behavior [2]–[5].

As MEMS technology had its origin in microelectronics industry, it is not surprising that a large variety of instruments can be found to test their electrical characteristics. On the opposite, relatively few tools are available to measure the mechanical behavior of microfabricated devices. We only mention here the Micro System Analyzer developed by Polytec Inc. [6], [7]. This product combines three different optical techniques that enable noncontact measurement of topography as well as 3-D dynamics of microstructures. Static characterization of surface topography is achieved by white-light interferometry. Out-of-plane vibration modes up to 24 MHz are extracted by a laser vibrometer which performs measurements on a grid of scan points [8], [9]. In-plane motion is computed by image analysis of videos taken with a standard charge-coupled device (CCD) camera combined with stroboscopic illumination [10]. Although its price remains prohibitive for most research laboratories, the performance of this state-of-the-art commercial instrument encompasses the specifications of most MEMS devices. It is also representative of recent noncontact techniques developed for measuring static and dynamic behaviors of MEMS, which are essentially based on optical methods [3]–[5], [11]–[17].

As this paper concerns in-plane motion analysis, we shall give a brief overview of the main optical methods used for in-plane measurements [3], [5], [13]. First, as a method not based on image analysis, one may consider using a laser-based principle. This can be achieved, for example, with a laser Doppler vibrometer (LDV) which uses the Doppler effect to measure the amount of vibration at a single point on an object's surface.

Manuscript received September 20, 2011; revised March 8, 2012; accepted March 12, 2012. Date of publication April 6, 2012; date of current version July 27, 2012. This work was supported by the Swiss National Science Foundation through Ambizione under Grant PZ00P2_121827. Subject Editor D. Elata.

C. Yamahata and M. A. M. Gijs are with the Laboratory of Microsystems, Institute of Microengineering, École Polytechnique Fédérale de Lausanne, 1015 Lausanne, Switzerland (e-mail: christophe.yamahata@a3.epfl.ch; martin.gijs@epfl.ch).

M. Stranczl was with the Laboratory of Microsystems, Institute of Microengineering, École Polytechnique Fédérale de Lausanne, 1015 Lausanne, Switzerland. He is now with Nivarox-FAR S.A., CH-2400 Le Locle, Switzerland (e-mail: marc.stranczl@a3.epfl.ch)

E. Sarajlic is with SmartTip B.V., 7522 NB Enschede, The Netherlands (e-mail: e.sarajlic@smarttip.nl).

G. J. M. Krijnen is with the MESA+, University of Twente, 7500 AE Enschede, The Netherlands (e-mail: gijs.krijnen@utwente.nl).

Color versions of one or more of the figures in this paper are available online at http://ieeexplore.ieee.org.

Digital Object Identifier 10.1109/JMEMS.2012.2191265

More precisely, it measures the projected component of the surface vibration vector along the direction of the incident laser beam. Thus, if aligned orthogonally to the surface under test, LDV measures exclusively the out-of-plane vibrations. While LDV is the most sensitive in this configuration, it can also be used to measure in-plane vibrations if the surface is tilted with respect to the laser beam. However, when in-plane amplitudes are larger than tens of nanometers, video microscopy associated with image processing techniques is more powerful [3]. Here, we may distinguish the existing techniques based on experimental parameters like: the video frame rate f_s, the light exposure duration δt, and the phase delay of the shutter ϕ with respect to the driving signal. With these parameters, we can essentially categorize these techniques as follows:

1) high-speed cinematography (f_s very large, δt very short, and $\phi = 0$) [18];
2) stroboscopic video microscopy (f_s small, δt very short, and $\phi = \phi(t)$);
3) recording with a conventional camera to measure the following:
   a) slow motion (f_s small, δt long, and $\phi = 0$) [19], [20];
   b) motion blur envelope (f_s small, δt very long, and $\phi = 0$) [21].

Aside from the critical frequency f_M or bandwidth of the oscillation signal, the choice of either of these methods depends on the nature of the phenomenon to be measured. High-speed cinematography is rather reserved for observing nonperiodic or nonrepeatable transient processes on a very short period of time [18], [22]. Conversely, stroboscopic video microscopy is suitable for measuring high-frequency periodic or reproducible transient responses. The current performance achieved with this technique typically allows measuring signal responses with up to 1-MHz bandwidth [6]. Fortunately, if the dynamic response is limited to several tens of kilohertz, the use of a conventional CCD camera is likely to be sufficient. In the motion blur technique proposed by Burns and Helbig [21], the amplitude of motion of a vibrating part can be obtained by comparing the blurry image recorded with continuous illumination (or long light exposure) with a reference image recorded at rest position. Measurement can be done on a sharp edge—where the contrast between the moving structure and the background is high—by fitting the brightness profile with an arcsine function. Although quantitative data can be obtained with the motion blur method (e.g., see [21], [23], and [24]), it is primarily a qualitative method that is mostly used to estimate the resonant frequency of MEMS devices [25].

To understand the role of each of the parameters introduced earlier, we come back to the working principle of stroboscopic imaging. A typical timing diagram illustrating the stroboscopic method is shown in Fig. 1 [10]. The device under test is excited with a sinusoidal actuation signal and oscillates at a frequency $f_M = 1/T_M$. The actuation signal generator—and thus the object motion—is synchronized with a stroboscopic light source. The duration of the strobe flash pulses δt is chosen sufficiently short to record unblurred images ($\delta t \ll T_M$). The camera shutter is, in turn, synchronized with the excitation and remains open until enough light has been collected. In the example in Fig. 1, two "frozen" images are used for each frame

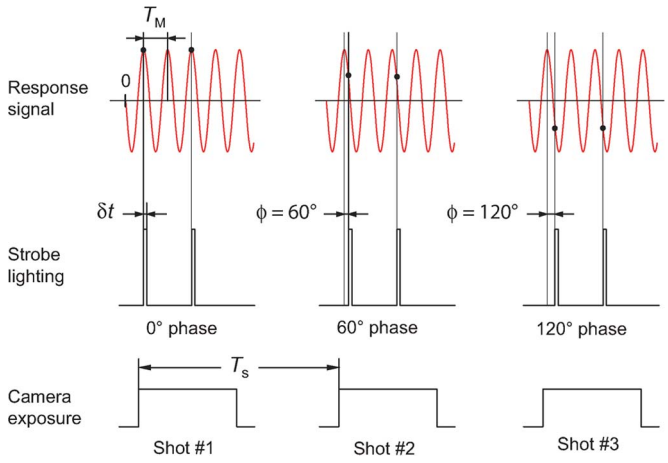

Fig. 1. Working principle of stroboscopic video microscopy. A sample is excited with a sinusoidal waveform generator which is synchronized with a strobe source. The sample vibrates at a frequency $f_M = 1/T_M$, which is much larger than the frame rate of the camera ($f_s = 1/T_s$). As the strobe generates ultrashort flashes of light (duration δt) synchronously with the phase position of the excitation signal (ϕ), the response signal can be perfectly reconstructed. In this timing diagram, the phase delay of the strobe illumination with respect to the response signal is incremented by $\Delta\phi = 60°$ after each frame shot.

shot. In order to reconstruct the motion of the moving object, after each frame shot, the flash pulses are shifted in time with a defined phase angle increment $\Delta\phi$. For example, in the timing diagram in Fig. 1, the motion is sampled at phase angles $\phi = 0°$, 60°, 120°, 180°, 240°, and 300°. As the camera has a limited frame rate ($f_s = (1/T_s) \ll f_M$), the device is seen to move with an apparent slow motion.

As emphasized in Fig. 1, the possibility of using multiple flash pulses of short duration to reconstruct a single shot is an important feature of the stroboscopic method. This allows one to keep a short integration time per sample, which is an essential parameter to be considered for large vibration frequencies (since the sampling duration acts as a low-pass filter of the signal). However, this capacity is obtained at the cost of an increased complexity due to the need for strobe lighting. For this reason, in what follows, the term "stroboscopy" is deliberately restricted to methods and instruments that intrinsically make use of a strobe, i.e., a shutter or an illumination source synchronized with the sample under test.[1]

While we have highlighted that high-frequency oscillating motions can be analyzed with a conventional camera ($f_s \ll f_M$) and an appropriate illumination scheme ($\delta t, \phi$), it should be noticed that one illumination scheme has not been exploited so far: short light exposures (with short or ultrashort delays δt) without any phase shifting ($\phi = 0$). This configuration is the opposite view of motion blur imaging and can be implemented very easily, simply by setting the camera shutter to a short aperture time. This case is the subject of this study. Hereafter, we demonstrate that a very simple and cost-effective video system, based purely on the theory of undersampling, can be used to extract in-plane amplitude responses of MEMS devices

[1]Following that logic, the "wagon-wheel effect" observed, for example, in a western movie would be simply described as a result of "temporal aliasing" because of being a direct consequence of the limited frame rate of the recorded media. Otherwise, if observed under stroboscopic conditions (e.g., flickering light), it would be explicitly called "stroboscopic effect."

for vibration frequencies of a few kilohertz. In the following sections, we explain the working principle of our method called "temporally aliased video microscopy" and demonstrate that it is suitable for experimental modal analysis of devices having either linear or nonlinear dynamic behavior. We start with a summary of the underlying theory of bandpass sampling (Section II). Next, we explain the principle of our undersampling method (Section III). Finally, we discuss the potential use of this method for the in-plane characterization of nonlinear systems (Section IV).

II. Undersampling of Bandpass Signals

Prior to detailing the principle of the proposed optical measurement method, it is worth recalling some basics of baseband- and bandpass-sampling theories. As we will see later, the "fanfold paper" representation presented in this section is particularly helpful in understanding frequency aliasing.

Baseband sampling: The Nyquist–Shannon sampling theorem states that, for a baseband signal $x(t)$ of bandwidth B, i.e., a signal whose continuous Fourier transform $X(f)$ occupies the interval of frequencies $f \in [-B, B]$, a sufficient condition for exact reconstructability of the signal from its digitized version is that the uniform sampling rate f_s must be chosen such that $f_s > 2B$ [26]. Thence, for a given sampling frequency f_s, the Nyquist criterion is respected as long as the signal occupies the positive baseband interval $[0, f_s/2)$. Here, it should be noticed that the dc component can be recovered because it contains trivial phase information [27]. The frequency $f_s/2$, sometimes denoted as f_N, is called the Nyquist frequency or folding frequency.

Bandpass sampling (undersampling): The Nyquist–Shannon theorem can be generalized to bandpass signals [27]. In that case, the condition for signal reconstructability is that $X(f) = 0$ outside the frequency bands $(-(n+1)(f_s/2), -n(f_s/2)) \cup (n(f_s/2), (n+1)(f_s/2))$ for all $n \in \mathbb{N}^*$. The positive frequency band, expressed as the interval $f \in [f_L, f_H]$, must be confined to the open interval $(n(f_s/2), (n+1)(f_s/2))$ since a frequency component at a multiple of the folding frequency $f_s/2$ would be impossible to retrieve.

Having noticed that the major difference between the samplings of baseband and bandpass signals is that baseband sampling can include the lowest frequency component ($f_L = 0$), we can give a general formulation of the Nyquist sampling criterion. For a band-limited signal $x(t)$ of bandwidth $B = f_H - f_L$, its continuous Fourier transform is such that

$$X(f) = 0 \qquad \forall f \notin [-f_H, -f_L] \cup [f_L, f_H]. \tag{1}$$

The sufficient condition for acceptable uniform sampling rates can be written [27]

$$\frac{f_H}{n} < \frac{f_s}{2} < \frac{f_L}{n-1}, \qquad \text{with } n \in \mathbb{N}^*; \quad n \leq \left\lfloor \frac{f_H}{B} \right\rfloor. \tag{2}$$

A simple representation of the Nyquist criterion is that of the "fanfold paper" shown in Fig. 2 [28]. The magnitude $|X(f)|$ of the positive frequency spectrum is "printed" on fanfold paper sheets which fold down at multiples of the frequency $f_s/2$, the so-called "folding" frequency. Signals above $f_s/2$ are folded down into sheet number 1, aliasing all the frequencies between zero and $f_s/2$. If the positive frequency spectrum of a bandpass signal entirely fits into a single sheet (either odd or even), excluding its edges, the sampled spectrum is just a low-frequency alias of the original spectrum, and signal reconstruction is possible. What Fig. 2 also shows is that, for even sheets number $2m$ ($m \in \mathbb{N}^*$), the downward frequency translation is further accompanied with a spectral reversal.

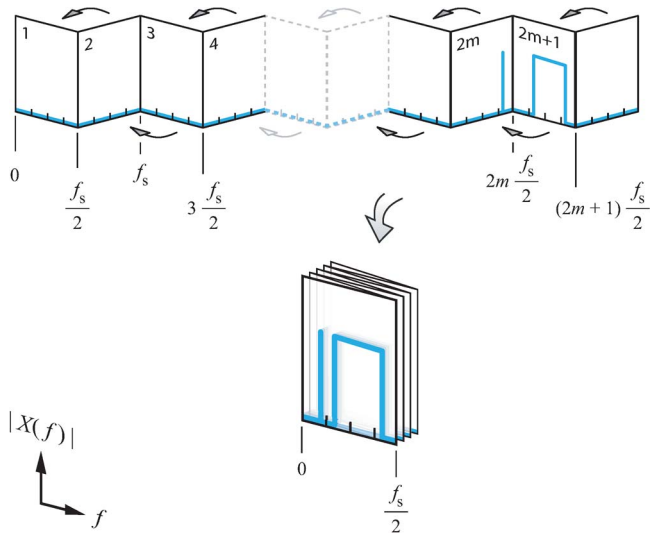

Fig. 2. Undersampling causes aliasing of the signal. This is best illustrated with the fanfold paper method [28]. In this illustration, the sampling frequency is f_s. All positive signal frequencies above the folding frequency $f_s/2$ are folded down into the band between zero and $f_s/2$.

The fanfold representation of the negative frequency spectrum is the mirrored version of Fig. 2, in which the negative frequencies below $-f_s/2$ are folded into the band between $-f_s/2$ and zero. The signal frequencies in the open interval $(-(f_s/2), f_s/2)$—and, in particular, the dc component—are not folded down. Thus, the fanfold paper method suitably illustrates the Nyquist sampling criterion for both baseband and bandpass signals.

III. Temporally Aliased Video Microscopy

We call our measurement method "temporally aliased video microscopy" because it takes advantage of the theory of undersampling (summarized in Section II) to perform in-plane experimental modal analysis of MEMS with a conventional CCD camera. Unlike stroboscopic methods, which, by definition, require the use of a synchronized stroboscopic shutter or light source, temporally aliased video microscopy only makes use of the embedded shutter of a CCD camera.[2] This simplifies considerably the experimental setup since no synchronization is needed between the excitation signal generator and the video recording equipment.

[2]Note that several architectures are possible for implementation of the CCD image sensor, for which distinct approaches correspond to the problem of shuttering (i.e., either with a mechanical or an electronic shutter). Here, we assume a global shuttering approach in which the entire frame is exposed for the same time window.

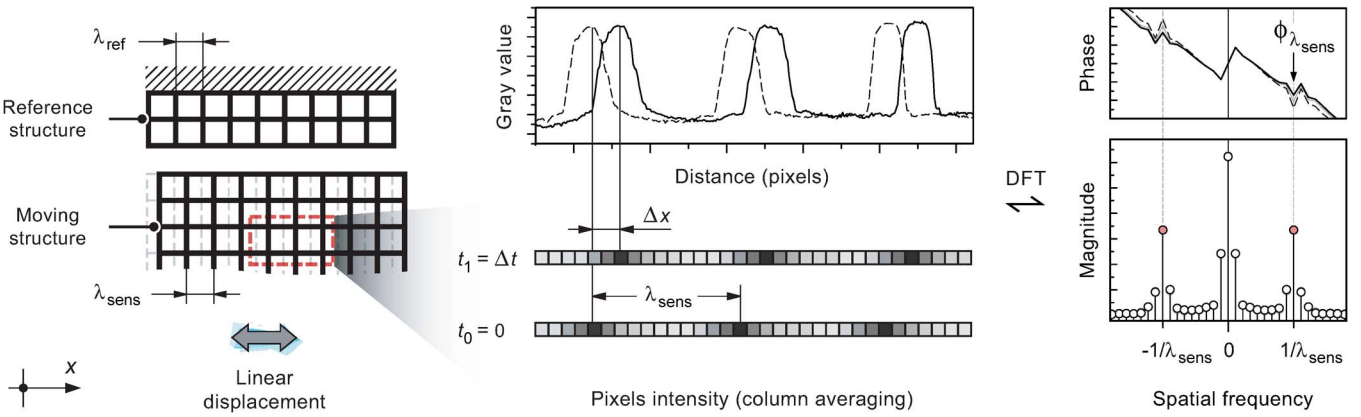

Fig. 3. Principle of the in-plane translation measurement method [20]. A CCD camera attached to a microscope simultaneously records periodic patterns of a reference and of a moving structure (spatial periods λ_{ref} and λ_{sens}, respectively). The motion-induced change in gray scale of pixels yields the displacement Δx, as calculated using DFT phase shifting. The dashed and full lines in the upper right panel correspond to the phase obtained from the pixel gray values at times t_0 and t_1, respectively. The displacement Δx is directly obtained from the phase change $\phi_{\lambda_{\mathrm{sens}}}$ calculated at the spatial frequency $1/\lambda_{\mathrm{sens}}$.

TABLE I
CONFIGURATION OF THE OPTICAL MEASUREMENT SETUP

Equipment / Parameter	Model / Specifications
Digital microscope	Keyence VHX-600E
Zoom lens	VH-Z500R (×5000[a])
Video	Windows AVI; progressive scan; 800 px × 480 px; 256 levels of gray (8-bit)
Selectable frame rates	15 fps / 28 fps
Shutter aperture time	1/5000 s (min. value)

[a] Ratio between the apparent size on the 15-inch LCD monitor of the digital microscope and the true size.

A. Image Processing Algorithm and Optical Measurement Setup

Temporally aliased video microscopy may be applicable with any image processing algorithm capable to retrieve position or orientation data from an image. Hereafter, we have used a simple algorithm that we have recently proposed for static characterization of MEMS [20], [29]. For the sake of clarity, the working principle of that method is shown in Fig. 3. Briefly, a MEMS device featuring periodic micropatterns is observed with a CCD camera attached to an optical microscope. Translation of the microstructure in the x-direction is retrieved from the comparison of two images by discrete Fourier transform (DFT) analysis using phase-shift computation.

For all the experiments presented in this paper, the videos were recorded with a digital microscope VHX-600 (Keyence Corporation, Japan) whose main parameters are summarized in Table I. Their analysis was performed with the DFT measurement method, using the graphical user interface (stand-alone MATLAB GUI) freely downloadable from our institutional Web site [29], [30].

B. Push–Pull Electrostatic Actuator

The experiments discussed in Section III were performed on push–pull electrostatic comb-drive devices using the driving circuit shown in Fig. 4. It is noteworthy to mention that this is

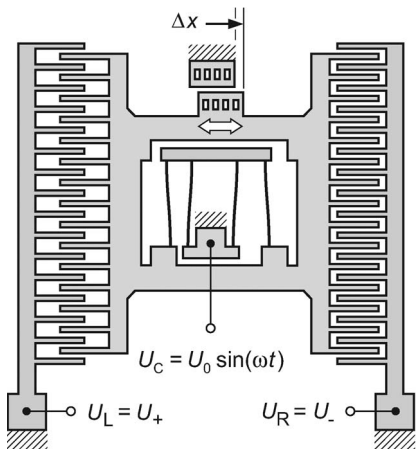

Fig. 4. Schematic of a push–pull comb-drive actuator and its driving scheme. Two dc power supplies (U_+, U_-) are connected to the left and right fixed combs (potentials U_L and U_R, respectively), while an ac power supply $(U_0 \sin(\omega t))$ is connected in the center to the moving combs (potential U_C).

probably the most commonly used type of microactuator for the design of silicon-based MEMS devices [25], [31]–[34]. While several driving schemes are possible for such a device (see, in particular, [34]), our driving circuit is particularly suitable for dynamic analysis. Indeed, it only requires two dc power supplies and one ac function generator. The driving potentials on the left and right fixed combs are denoted as U_L and U_R, respectively. They were set precisely to $U_L = U_+$ and $U_R = -U_L = U_-$ using a multiple-output dc power supply (GPS-3303, GW Instek, Taiwan). The moving combs were set to the same ac potential $U_C(t) = U_0 \sin(\omega t)$, using an arbitrary waveform generator (Agilent 33250A) driving a high-voltage amplifier (WMA-280, Falco Systems, The Netherlands).

The electrostatic force $F_x(t)$ associated with this driving circuit is

$$F_x(t) = \frac{1}{2}\frac{\partial C}{\partial x}\left((U_R - U_C)^2 - (U_L - U_C)^2\right)$$
$$= 2\frac{\partial C}{\partial x} U_+ \cdot U_0 \sin(\omega t) \quad (3)$$

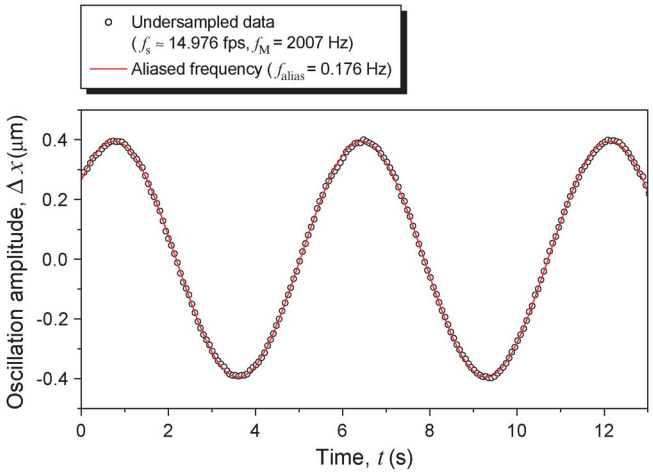

Fig. 5. Illustration of the frequency aliasing caused by undersampling. In this experiment, the motion of a push–pull actuator oscillating at 2007 Hz was recorded at a frame rate of 14.976 frames/s, setting the shutter aperture time to 1/5000 s. As a result, the device motion was observed with an apparent frequency of 0.176 Hz.

where x is the lateral displacement of the structure and C is the capacitance of each pair of comb drives (assumed to be perfectly balanced, and identical for $x = 0$). For interdigitated comb electrodes and small displacements, $\partial C/\partial x$ is a constant [31]. As a result, the force is directly proportional to the ac driving voltage $U_C(t)$ and can be rewritten as

$$F_x(t) = F_0 \sin(\omega t), \qquad \text{with } F_0 = 2\frac{\partial C}{\partial x} U_+ \cdot U_0. \quad (4)$$

Assuming linear spring and damping, the equation of motion of the push–pull electrostatic actuator is given by the linear differential equation

$$\ddot{x} + 2\xi\omega_0\dot{x} + \omega_0^2 x = \frac{F_0}{M}\sin(\omega t) \quad (5)$$

where ξ is the damping ratio, M is the effective mass of the moving structure, ω_0 is the undamped angular frequency, and F_0 is the amplitude of the driving force given in (4).

C. Frequency Aliasing

In signal sampling theory, aliasing refers to the phenomenon whereby a periodic signal is not faithfully represented in the sampled signal due to undersampling. Let us describe aliasing mathematically considering a sinusoidal signal of frequency f_M. When sampled at a frequency $f_s < 2f_M$, while ensuring that f_M is not a multiple of the folding frequency $f_s/2$ (see Fig. 2), the resulting samples become indistinguishable from those of another sinusoidal signal of frequency

$$f_{\text{alias}}(n) = \left| f_M - n\frac{f_s}{2} \right| \qquad \forall n \in \mathbb{N}. \quad (6)$$

By default, the smallest of these frequencies would be used to reconstruct the signal, leading to an erroneous reconstruction (or aliasing artifact). An illustrative example is shown in Fig. 5. For this experiment, a comb-drive microactuator was excited with a pure sine voltage. The oscillation frequency of the device was set precisely to $f_M = 2007$ Hz, and the video was recorded at a rate of $f_{s,1} \approx 15$ frames/s. In order to capture unblurred images, we have used a shutter aperture time $\delta t = 1/5000$ s. After analysis of the video, we could fit the data with a sine wave and extract the aliased frequency $f_{\text{alias}} = 0.1758$ Hz. From (6), we deduce that the actual video frame rate was $f_{s,1} = 14.9763$ frames/s (with $n = 268$).[3]

In order to perform in-plane dynamic characterization of this MEMS device, one could imagine repeating the experiment for various excitation frequencies f_M, spanning the frequency range of interest, except at multiples of the folding frequency

$$f_M \in \mathbb{R}_+ \setminus \left\{ n\frac{f_s}{2}, n \in \mathbb{N}^* \right\}. \quad (7)$$

As discussed in the following section, we can actually greatly simplify the video treatment by proceeding, instead, with a series of band-limited signals that satisfy (1) and (2). That is, to refer to the fanfold paper representation, the frequency response function can be retrieved by performing "sheet-by-sheet" undersamplings.

D. Chirp Signal Undersampling

A chirp is a signal in which the frequency is swept with time, either upward or downward. The sinusoidal linear chirp $u(t)$ is defined as

$$u(t) = \begin{cases} U \sin\left[2\pi\left(f_L + \frac{\Delta f}{2T}t\right)t\right], & \text{if } 0 \le t \le T \\ 0, & \text{if } t \notin [0, T] \end{cases} \quad (8)$$

where U is the amplitude, f_L is the starting frequency, Δf is the frequency bandwidth, T is the chirp duration, $\Delta f/T$ is the chirp rate, and t is the time. The instantaneous frequency of the chirp function $u(t)$ is

$$f(t) = \frac{1}{2\pi}\frac{d}{dt}\left[2\pi\left(f_L + \frac{\Delta f}{2T}t\right)t\right], \qquad \text{if } 0 \le t \le T$$
$$= f_L + \frac{\Delta f}{T}t. \quad (9)$$

In practice, the sinusoidal chirp of (8) is not band limited because the signal is time limited. Nevertheless, good interpolation results can be achieved if the chirp duration is much greater than the sampling period

$$T \gg T_s, \qquad \text{where } T_s = \frac{1}{f_s}. \quad (10)$$

To satisfy this condition (which is *a fortiori* satisfied if $(1/T) \ll (f_s/2)$) as well as the Nyquist criterion $(\Delta f < (f_s/2))$,

[3]The Keyence Digital Microscope VHX-600 used for our measurements is primarily aimed for high-definition imaging. The recording frame rate—indicated to be 15 frames/s (28 frames/s in higher speed recording mode) according to technical specifications—was found to be 14.976 frames/s (27.781 frames/s in higher speed mode) for our equipment. A sales engineer from Keyence confirmed that the frame rate is a parameter that is not tuned during factory configuration and can thus vary from one instrument to another.

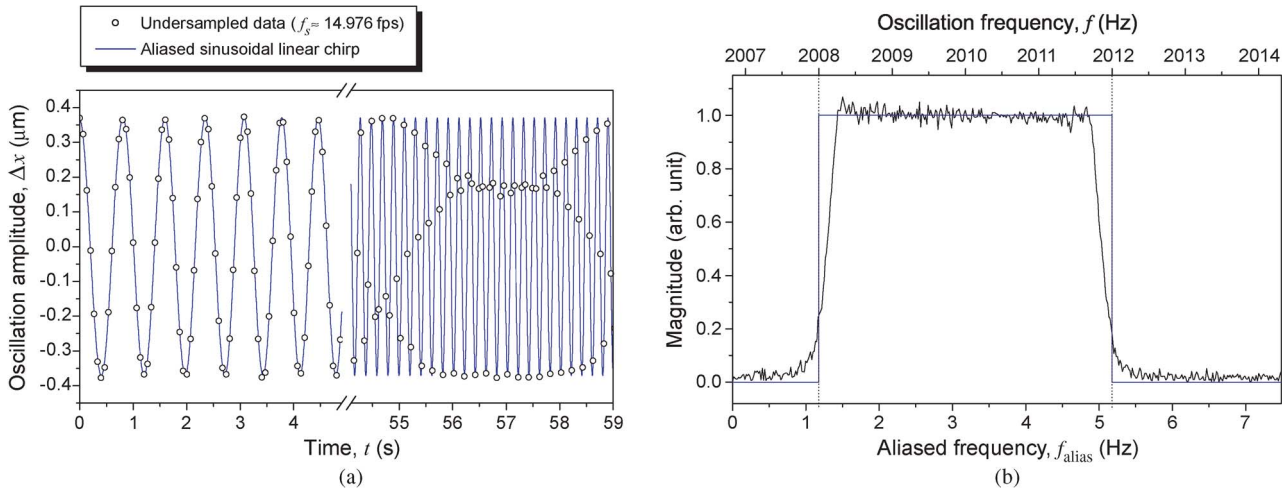

Fig. 6. Illustration of the aliasing of a band-limited sinusoidal chirp caused by undersampling. In this experiment, a push–pull actuator was excited with a linear chirp increasing between 2008 and 2012 Hz in 60 s. The motion was recorded at a frame rate of 14.976 frames/s, setting the shutter aperture time to 1/5000 s. As a result, the device motion was observed with an apparent frequency increasing between 1.176 and 5.176 Hz. In (a), we show the measurement data extracted from the video analysis. The results are fitted with (solid line) an aliased sinusoidal chirp. In (b), we show the computed frequency spectrum of these measurements: To attenuate spectral leakage, the data were temporally windowed with a trapezoidal function prior to fast Fourier transform operation. The aliased and actual frequency spectrums are given in the lower and upper horizontal axes, respectively.

the chirp rate should be chosen sufficiently low to ensure that

$$\frac{\Delta f}{T} \ll \left(\frac{f_s}{2}\right)^2. \tag{11}$$

To illustrate undersampling of a chirp signal, the push–pull electrostatic actuator used in the previous experiment was excited with a sinusoidal linear chirp. In the experimental results shown in Fig. 6, we have used the following parameters: $f_L = 2008$ Hz, $\Delta f = 4$ Hz ($f_H = 2012$ Hz), $T = 60$ s, and $f_s = f_{s,1} = 14.9763$ frames/s. With these parameters, the excitation spectrum entirely fits into the odd sheet number 269 in the fanfold representation in Fig. 2. Also, since the excitation frequency bandwidth is short and happens to be far from the resonant frequency of the device, we can approximate the oscillation amplitude of the microactuator as a constant in this frequency range.

The results shown in Figs. 5 and 6 illustrate how *a priori* knowledge of the frequency range of a band-limited signal could be exploited for accurate signal reconstruction from its digitized version. In particular, these results could be used for plotting the frequency response function of the MEMS device, i.e., the magnitude of the displacement as a function of the oscillation frequency.

E. Sampling Theorem Infringement

So far, we have been cautious to fulfill the Nyquist–Shannon sampling theorem when selecting the band-limited excitation signals. More particularly, we have warned the reader that signal frequencies at multiples of the folding frequency would be impossible to reconstruct [see (7)]. Let us see what actually occurs when we infringe the sampling theorem. For the following experiment, we have used a push–pull microactuator with an integrated differential capacitive sensor. The MEMS device was excited with a sinusoidal linear chirp, increasing the frequency between $f_L = 0$ Hz (dc excitation) and $f_H = 1000$ Hz in $T = 180$ s. The motion was recorded at two different frame rates $f_{s,1} = 14.976$ frames/s and $f_{s,2} = 27.781$ frames/s, setting the shutter aperture time to $\delta t = 1/5000$ s. The video measurements are shown in Fig. 7(a) and compared with those of the solid-state capacitive sensor. The latter were obtained with a commercial integrated circuit (MS3110 Universal Capacitive Readout, Irvine Sensors Corporation) [35]. With both measurements, we find that the resonant frequency of the device is $f_r = 450$ Hz. In addition, we clearly see from the data obtained by temporally aliased video microscopy that the system behaves as a driven harmonic oscillator. From the envelopes of the optical measurement data, we could retrieve the damping ratio $\xi = 0.13$ (quality factor $Q \approx 4$) and the amplitude of the frequency response, thus finding the parameters of the differential equation (5). Indeed, the frequency response of a harmonic oscillator is

$$X(f) = \frac{X_0}{\sqrt{\left(1-\left(\frac{f}{f_0}\right)^2\right)^2 + \left(2\xi\frac{f}{f_0}\right)^2}}, \qquad X_0 = \frac{F_0}{M\omega_0^2} \tag{12}$$

where f is the actuation frequency ($f = \omega/2\pi$), X_0 is the amplitude measured for dc actuation ($f = 0$), and f_0 is the natural frequency ($f_0 = \omega_0/2\pi$).[4]

The frequency response shown in Fig. 7(a) is not, strictly speaking, a frequency spectrum (i.e., it is not the result of a mathematical transformation from time to frequency domain). Thus, contrary to the windowing operation used to perform spectral analysis [see Fig. 6(b)], temporally aliased video microscopy is, by nature, free from spectral leakage. The only "leakage" that it has to deal with is frequency folding, and we will see how we can actually take advantage of it.

[4]Note that we have an underdamped oscillator ($\xi < 1$). With $\xi = 0.13$, we can assume the resonant frequency (driving frequency for which the amplitude response is maximum) f_r to be identical to the natural frequency: $f_r = f_0\sqrt{1-2\xi^2} \approx f_0$; $X(f_r) = Q \cdot X_0$.

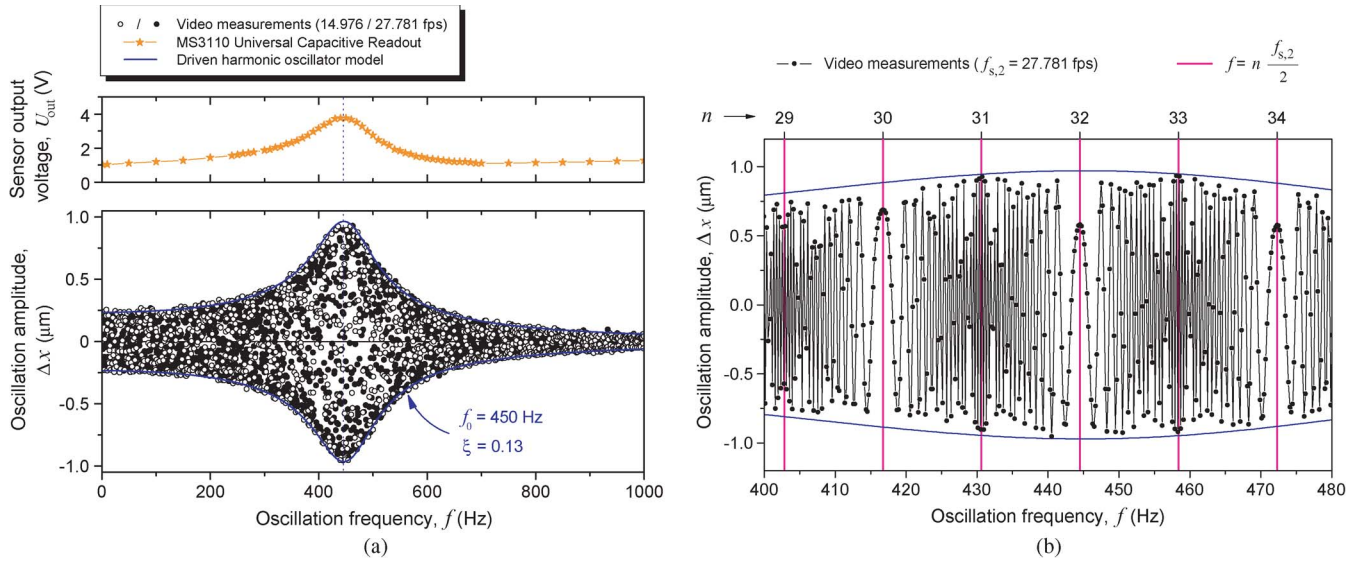

Fig. 7. Dynamic characteristics of a push–pull electrostatic actuator. In (a), (upper graph) the electrical measurements obtained with a solid-state differential capacitive sensor are compared with (lower graph) those obtained optically by "temporally aliased video microscopy" at frame rates $f_{s,1} = 14.976$ frames/s and $f_{s,2} = 27.781$ frames/s. The MEMS device has the linear characteristic of a damped harmonic oscillator, with a resonant frequency at 450 Hz and a damping coefficient of 0.13 (corresponding to a low Q factor of four). The graph in (b) is a close-up view of the measurement data shown in (a) for the sampling frequency $f_{s,2} = 27.781$ frames/s. Stroboscopic "freezing" is observed for signal frequencies at even multiples of the folding frequency, at $f = n(f_{s,2}/2)\ \forall n \in 2\mathbb{N}^*$.

To better understand why temporally aliased video microscopy enables dynamic characterization, we shall examine more closely the results in Fig. 7(a). In Fig. 7(b), we show a close-up view of the experimental data measured at frame rate $f_{s,2} = 27.781$ frames/s, around the resonant frequency of the MEMS device. The graph shows regular nodes: When the device oscillation frequency approaches a multiple n of the folding frequency, the sampled signal appears to be "frozen." More precisely, we can observe that the sampled signal appears to be alternatively "bistable" (two distinct levels) and "frozen" (one single level) at odd and even values of n, respectively. These stroboscopic artifacts occur because of frequency aliasing and are well explained by (6). Even though the signal cannot be reconstructed at multiples of the folding frequency, these nodes can be helpful in data treatment. Indeed, since we use a sinusoidal chirp wave for the excitation, the instantaneous frequency of the response is known. Therefore, the function generator used for the excitation does not need to be synchronized with the CCD camera because the nodes can serve to match a given video frame with the corresponding instantaneous excitation frequency.

Before concluding this section, we need to consider the case where the critical signal information happens to be exactly at a multiple of the folding frequency. For example, this happens if a system with a high Q factor has its resonant frequency close to the folding frequency. A simple solution to prevent this occurrence is to use a CCD camera with at least two selectable frame rates $f_{s,1}$ and $f_{s,2}$ which must be such that there is no overlap of their folding frequencies in the frequency range of interest $[f_L, f_H]$

$$n\frac{f_{s,1}}{2} \neq m\frac{f_{s,2}}{2}, \qquad \text{with } n, m \in \mathbb{N}^* \qquad \forall n\frac{f_{s,1}}{2} \in [f_L, f_H]. \tag{13}$$

Obviously, this condition is always satisfied if $f_{s1}/f_{s,2}$ is an irrational number.

IV. Dynamic Characterization of Nonlinear Systems

In the previous section, in the discussion of forced vibrations, we have assumed that the system's vibration frequency is the same as that of the disturbing force. In this section, we discuss the cases where vibrations may appear at multiples or fractions of the excitation frequency. These phenomena are known as superharmonic and subharmonic resonances, respectively [36].

A. Electromechanical Subharmonic Resonant System

Subharmonic resonance may occur in any pronounced nonlinear system with small effective damping [36], [37]. The system studied in this section is schematically shown in Fig. 8. It consists of a cantilever of stiffness K with an end mass M that is made to swing by an electrostatic actuator [excited with sinusoidal voltage $U(t)$]. This nonautonomous system has a damping ratio ξ and is described by the nonlinear differential equation [38]

$$\ddot{x} + 2\xi\omega_0\dot{x} + \omega_0^2 x = -\Gamma \sin\left(\omega_x x - \frac{2\pi}{3}\right) U^2(t) \tag{14}$$

where $\omega_0 = \sqrt{K/M}$, $\omega_x = 2\pi/\lambda_x$, $\Gamma = \Delta C\omega_x/2M$, and ΔC is the amplitude of capacitance variations. In this model, we have made the assumption that the spatial capacitance variation $\partial C/\partial x$ can be approximated by a sine with angular wavenumber ω_x. Equation (14) is, in fact, the equation of motion of a frictionless three-phase electrostatic stepper micromotor with only one phase "on." A thorough analysis of the dynamics of this micromotor is presented elsewhere [39].

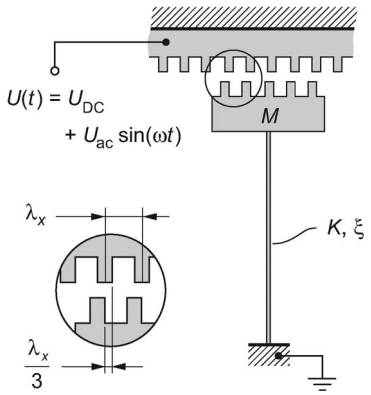

Fig. 8. Schematic of the nonlinear electromechanical resonant device. The mass M can be made to vibrate at angular frequency $\omega_0 = \sqrt{K/M}$ by an exciting force of lower or higher frequency (respectively $\omega_0/2$ and $2\omega_0$ in the cases described in Section IV).

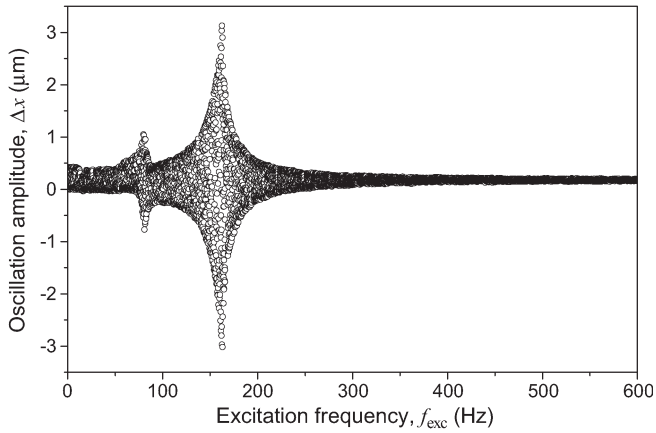

Fig. 9. Dynamic characterization of a microactuator excited with a sinusoidal signal (angular frequency $\omega = 2\pi f_{\rm exc}$) containing a harmonic wave at 2ω. Temporally aliased video microscopy was performed at a frame rate $f_{s,1} = 14.976$ frames/s. For this experiment, we have used a linearly increasing sinusoidal chirp with $U_{\rm dc} = 1$ V and $U_{\rm ac} = 0.5$ V. The resonant frequency of the device is $f_0 = 163$ Hz. Superharmonic vibration occurs for $f_{\rm exc} = f_0/2$.

B. Harmonics and Resonance

As a preliminary to the discussion on harmonic resonance, let us consider the simple case of a system subjected to an "impure" sine wave. The excitation signal may be described as a Fourier series containing harmonics $nf_{\rm exc}$ at multiples $n \in \mathbb{N}^*$ of the fundamental frequency $f_{\rm exc}$. Thus, we may observe resonance of the system caused by these higher harmonics. An easy implementation of this resonance artifact consists in exciting the system shown in Fig. 8, with a sine wave containing a dc bias

$$U(t) = U_{\rm dc} + U_{\rm ac}\sin(\omega t) \tag{15}$$

with $U_{\rm dc}$ as the dc bias voltage and $U_{\rm ac}$ as the amplitude of the sine wave. Since the electrostatic force varies quadratically with $U(t)$, it is helpful to rewrite $U^2(t)$ as

$$U^2(t) = \left(U_{\rm dc}^2 + \frac{1}{2}U_{\rm ac}^2\right) + 2U_{\rm dc}U_{\rm ac}\sin(\omega t) - \frac{1}{2}U_{\rm ac}^2\cos(2\omega t). \tag{16}$$

From (16), we see that the excitation signal contains two sine waves with angular frequencies ω and 2ω. In Fig. 9, we show a typical measurement performed on the microactuator shown in Fig. 8 and subjected to an excitation of the form given in (16), with $U_{\rm dc} = 1$ V and $U_{\rm ac} = 0.5$ V. Using a waveform generator, the system was subjected to a linearly increasing sinusoidal chirp. The natural frequency of the system is found at $f_0 = 163$ Hz, and superharmonic resonance can be observed around the excitation frequency $f_{\rm exc} = f_0/2$. Although this example is relatively simple, it demonstrates that temporally aliased video microscopy can be used to identify resonance peaks occurring at frequencies distinct from the fundamental frequency of the excitation.

C. Superharmonics and Subharmonics in Nonlinear Systems

The trivial example described before brings us to the general characterization of nonlinear systems which are, in essence, complicated to analyze [40]–[44]. In nonlinear systems, forced excitation with a pure sinusoidal waveform may generate superharmonic and subharmonic resonances [44]. While superharmonic resonance is not specific to nonlinear systems, subharmonic resonance is clearly a signature of nonlinearity.

Eliminating the dc bias in (16) and introducing $\Omega = 2\omega$ as the angular excitation frequency, (14) becomes

$$\ddot{x} + 2\xi\omega_0\dot{x} + \omega_0^2 x = -\Gamma\frac{U_{\rm ac}^2}{2}\sin\left(\omega_x x - \frac{2\pi}{3}\right)(1 - \cos(\Omega t)). \tag{17}$$

Suppose now that $x(t)$ is a solution with angular frequency ω [37]. Then, $x(t)$ can be represented by a Fourier series for all t

$$x(t) = a_0 + a_1\cos(\omega t) + b_1\sin(\omega t) + a_2\cos(2\omega t) + \cdots \tag{18}$$

where $a_0, a_1, b_1, a_2, \ldots$ are constant coefficients. If we substitute this series into (17), the term $\sin(\omega_x x(t) - (2\pi/3))$ is also periodic and so generates another Fourier series. The right term in (17) may then be developed using the substitutions

$$\begin{aligned}\sin(n\omega t)\cos(\Omega t) &= \frac{1}{2}\left(\sin(n\omega t + \Omega t) + \sin(n\omega t - \Omega t)\right)\\ \cos(n\omega t)\cos(\Omega t) &= \frac{1}{2}\left(\cos(n\omega t + \Omega t) + \cos(n\omega t - \Omega t)\right)\end{aligned} \tag{19}$$

for all $n \in \mathbb{N}^*$. Matching the two sides of (17) then gives a set of equations for $a_0, a_1, b_1, a_2, \ldots$ and enables ω to be determined. An obvious solution is $\omega = \Omega$, but the matching may also be achieved when

$$\omega = \frac{\Omega}{n}, \qquad \text{with } n \in \mathbb{N}^*. \tag{20}$$

These are called subharmonics of order $1/n$. Such a phenomenon can be clearly observed in the experimental data in Fig. 10 where, in addition to the superharmonic observed for $\Omega = \omega_0/2$, a subharmonic is clearly visible for $\Omega = 2\omega_0$ (i.e., $\omega = (\Omega/2) = \omega_0$). In the latter case, we expect the response signal to consist of two main sinusoidal waves: one

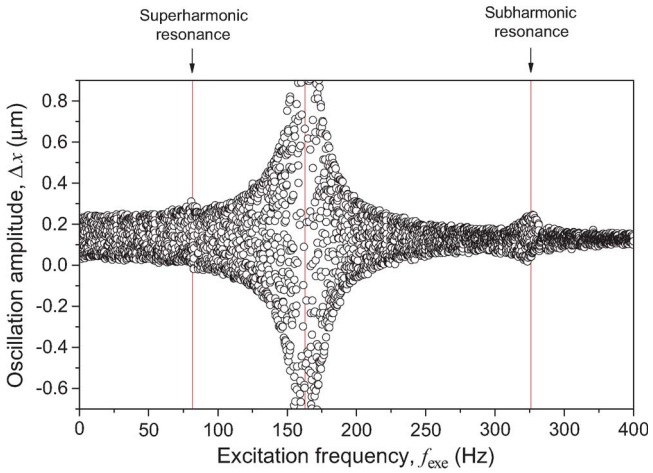

Fig. 10. Superharmonic and subharmonic resonances are observed on a nonlinear system characterized by temporally aliased video microscopy. The graph was obtained with a linearly increasing sinusoidal chirp (angular frequency $\Omega = 2\pi f_{\rm exc}$) with $U_{\rm ac} = 2$ V. The resonant frequency of the device is $f_0 = 163$ Hz. Superharmonic vibration occurs for $f_{\rm exc} = f_0/2$. Subharmonic vibration can also be observed for $f_{\rm exc} = 2f_0$.

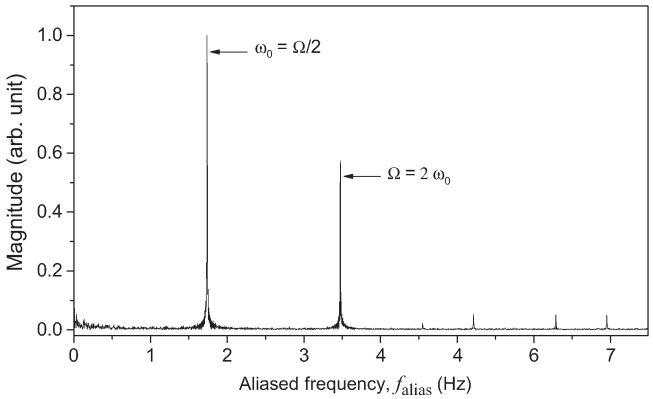

Fig. 11. Aliased frequency spectrum discloses subharmonic resonance. The measurement was performed with an excitation frequency of $f_{\rm exc} = 2f_0 = 326$ Hz (angular frequency $\Omega = 2\pi f_{\rm exc}$). The two main peaks are aliased frequencies corresponding to subharmonic resonance (ω_0) and excitation frequency (Ω).

at the excitation frequency (Ω) and the other at the subharmonic resonant frequency of order $1/2$ $(\omega = \Omega/2)$. To verify this hypothesis, we have excited the system at about twice its natural frequency $(f_{\rm exc} = 2f_0 = 326$ Hz) and performed temporally aliased video microscopy at a frame rate $f_{s,1} = 14.9763$ frames/s. The aliased frequency spectrum is shown in Fig. 11. Two peaks stand out clearly from the rest of the spectrum at $f_{\rm alias,1} \approx 1.74$ Hz and $f_{\rm alias,2} \approx 3.48$ Hz. Remembering the fanfold paper representation in Fig. 2 and using (6), we can deduce that these peaks correspond to frequencies $f_{M,1} = f_0 = 163$ Hz and $f_{M,2} = 2f_0 = 326$ Hz, respectively. Note that the other peaks correspond to frequency aliases of higher harmonics. Similar results could be achieved at frame rate $f_{s,2} = 27.781$ frames/s. Furthermore, we could validate our hypothesis with a high-speed camera [39].

Before closing the discussion on the characterization of nonlinear systems, we draw the reader's attention to the fact that we have only presented amplitude–frequency responses for forward frequency sweeps. As we also performed experiments with backward frequency sweeps, we could observe noticeable hystereses between forward and backward responses as well as "jump effects," particularly in the region of subharmonic resonance. These features are other typical signatures of nonlinear systems that can be easily evidenced by temporally aliased video microscopy.

V. Conclusion

We have proposed temporally aliased video microscopy as a powerful optical method for the study of in-plane vibrations in MEMS devices from videos recorded with a conventional CCD camera (i.e., having a typical recording frame rate of about 28 frames/s). Quantitative measurements of resonant frequencies, with resolutions better than 1 Hz, could be extracted from video microscopy of systems having in-plane vibration modes in the range of hundreds of hertz to a few kilohertz. The upper frequency limit is not dictated by the frame rate but is a matter of aperture duration of the shutter and sensitivity of the CCD image sensor [13]. Thus, while we have performed our measurements using a relatively long shutter aperture time (1/5000 s), our method can theoretically be used to analyze devices with much higher bandwidths than those presented in this paper. Indeed, as shown in Fig. 5, we succeed to measure high vibration amplitudes as long as the velocities are low enough to capture unblurred (or with limited blur) video frames. Last but not least, our method has proven to be efficient for the characterization of linear and nonlinear systems. In particular, we could demonstrate that the method enables the disclosure of superharmonic and subharmonic resonance features.

Temporally aliased video microscopy advantageously complements current optical methods used for MEMS in-plane dynamic characterization. For MEMS devices with linear frequency response function in the range of several hundreds of kilohertz and up to 1 MHz, stroboscopic video microscopy is certainly the best choice. To observe nonrepeatable transient processes, high-speed cinematography must be chosen. Fortunately, in all other cases, the use of a conventional camera is proven to be sufficient. At first, for a quick yet qualitative search of the resonant peaks in the frequency range of a few kilohertz, the "blur envelope" approach happens to be sufficient. Then, if accurate quantitative data are desired, or when nonlinearities are observed, temporally aliased video microscopy is a more efficient method.

References

[1] J. L. Hutter and J. Bechhoefer, "Calibration of atomic-force microscope tips," *Rev. Sci. Instrum.*, vol. 64, no. 7, pp. 1868–1873, Jul. 1993.
[2] D. M. Freeman, "Measuring motions of MEMS," *MRS Bull.*, vol. 26, no. 4, pp. 305–306, Apr. 2001.
[3] A. Bosseboeuf and S. Petitgrand, "Characterization of the static and dynamic behaviour of M(O)EMS by optical techniques: Status and trends," *J. Micromech. Microeng.*, vol. 13, no. 4, pp. S23–S33, Jul. 2003.
[4] O. B. Ozdoganlar, B. D. Hansche, and T. G. Carne, "Experimental modal analysis for microelectromechanical systems," *Exp. Mech.*, vol. 45, no. 6, pp. 498–506, Dec. 2005.
[5] R. M. Lin and W. J. Wang, "Structural dynamics of microsystems—Current state of research and future directions," *Mech. Syst. Signal Process.*, vol. 20, no. 5, pp. 1015–1043, Jul. 2006.
[6] Polytec MEMS Analyzers. [Online]. Available: http://www.polytec.com/microsystems/

[7] M. Stranczl, E. Sarajlic, G. J. M. Krijnen, H. Fujita, M. A. M. Gijs, and C. Yamahata, "Modal analysis and modeling of a frictionless electrostatic rotary stepper micromotor," in *Proc. 24th IEEE MEMS*, Cancún, Mexico, Jan. 23–27, 2011, pp. 1257–1260.
[8] P. Avitabile, "Experimental modal analysis: A simple non-mathematical presentation," *Sound Vib.*, vol. 35, no. 1, pp. 20–31, 2001.
[9] *Polytec Tutorials: Optical Measurement and Vibrometry*. [Online]. Available: http://www.polytec.com/vib-university/
[10] E. M. Lawrence and C. Rembe, "MEMS characterization using new hybrid laser Doppler vibrometer/strobe video system," in *Proc. SPIE Rel., Test., Charact. MEMS/MOEMS III,* D. M. Tanner and R. Ramesham, Eds., San Jose, CA, Jan. 26, 2004, vol. 5343, pp. 45–54.
[11] J. S. Burdess, A. J. Harris, D. Wood, R. J. Pitcher, and D. Glennie, "A system for the dynamic characterization of microstructures," *J. Microelectromech. Syst.*, vol. 6, no. 4, pp. 322–328, Dec. 1997.
[12] M. R. Hart, R. A. Conant, K. Y. Lau, and R. S. Muller, "Stroboscopic interferometer system for dynamic MEMS characterization," *J. Microelectromech. Syst.*, vol. 9, no. 4, pp. 409–418, Dec. 2000.
[13] C. Rembe, R. Kant, and R. S. Muller, "Optical measurement methods to study dynamic behavior in MEMS," in *Proc. SPIE Microsyst. Eng., Metrol. Inspection,* C. Gorecki, W. P. O. Jüeptner, and M. Kujawínska, Eds., Munich, Germany, Jun. 20, 2001, vol. 4400, pp. 127–137.
[14] C. Rembe and R. S. Muller, "Measurement system for full three-dimensional motion characterization of MEMS," *J. Microelectromech. Syst.*, vol. 11, no. 5, pp. 479–488, Oct. 2002.
[15] B. Serio, J. J. Hunsinger, and B. Cretin, "In-plane measurements of microelectromechanical systems vibrations with nanometer resolution using the correlation of synchronous images," *Rev. Sci. Instrum.*, vol. 75, no. 10, pp. 3335–3341, Oct. 2004.
[16] P. Sandoz, J.-M. Friedt, and E. Carry, "In-plane rigid-body vibration mode characterization with a nanometer resolution by stroboscopic imaging of a microstructured pattern," *Rev. Sci. Instrum.*, vol. 78, no. 2, p. 023706, Feb. 2007.
[17] J. P. Gilles, S. Megherbi, G. Raynaud, F. Parrain, H. Mathias, X. Leroux, and A. Bosseboeuf, "Scanning electron microscopy for vacuum quality factor measurement of small-size MEMS resonators," *Sens. Actuators A, Phys.*, vol. 145–146, no. 1/2, pp. 187–193, Jul./Aug. 2008.
[18] C. Rembe, B. Tibken, and E. P. Hofer, "Analysis of the dynamics in microactuators using high-speed cine photomicrography," *J. Microelectromech. Syst.*, vol. 10, no. 1, pp. 137–145, Mar. 2001.
[19] P. Sandoz, V. Bonnans, and T. Gharbi, "High-accuracy position and orientation measurement of extended two-dimensional surfaces by a phase-sensitive vision method," *Appl. Opt.*, vol. 41, no. 26, pp. 5503–5511, Sep. 2002.
[20] C. Yamahata, E. Sarajlic, G. J. M. Krijnen, and M. A. M. Gijs, "Subnanometer translation of microelectromechanical systems measured by discrete Fourier analysis of CCD images," *J. Microelectromech. Syst.*, vol. 19, no. 5, pp. 1273–1275, Oct. 2010.
[21] D. J. Burns and H. F. Helbig, "System for automatic electrical and optical characterization of microelectromechanical devices," *J. Microelectromech. Syst.*, vol. 8, no. 4, pp. 473–482, Dec. 1999.
[22] J. P. Staforelli, E. Vera, J. M. Brito, P. Solano, S. Torres, and C. Saavedra, "Superresolution imaging in optical tweezers using high-speed cameras," *Opt. Exp.*, vol. 18, no. 4, pp. 3322–3331, Feb. 2010.
[23] S. Wang, B. Guan, G. Wang, and Q. Li, "Measurement of sinusoidal vibration from motion blurred images," *Pattern Recognit. Lett.*, vol. 28, no. 9, pp. 1029–1040, Jul. 2007.
[24] N. Ellerington, B. Bschaden, T. Hubbard, and M. Kujath, "Fourier analysis of blurred images for the measurement of the in-plane dynamics of MEMS," *J. Micromech. Microeng.*, vol. 22, no. 3, p. 035019, Mar. 2012.
[25] D. M. Tanner, A. C. Owen, Jr., and F. Rodriguez, "Resonant frequency method for monitoring MEMS fabrication," in *Proc. SPIE Rel., Test., Charact. MEMS/MOEMS II,* R. Ramesham and D. M. Tanner, Eds., San Jose, CA, Jan. 27, 2003, vol. 4980, pp. 220–228.
[26] C. E. Shannon, "Communication in the presence of noise," *Proc. IEEE*, vol. 86, no. 2, pp. 447–457, Feb. 1998.
[27] R. G. Vaughan, N. L. Scott, and D. R. White, "The theory of bandpass sampling," *IEEE Trans. Signal Process.*, vol. 39, no. 9, pp. 1973–1984, Sep. 1991.
[28] R. H. Hosking, "How to use undersampling," EE Times India, 2006. [Online]. Available: http://www.eetindia.co.in/
[29] C. Yamahata, E. Sarajlic, M. Stranczl, G. J. M. Krijnen, and M. A. M. Gijs, "Subpixel translation of MEMS measured by discrete Fourier transform analysis of CCD images," in *Proc. 16th TRANSDUCERS*, Beijing, China, Jun. 5–9, 2011, pp. 1697–1700.
[30] The MATLAB GUI can be downloaded free of charge. [Online]. Available: http://lmis2.epfl.ch/nanoplus/
[31] W. C. Tang, T.-C. H. Nguyen, and R. T. Howe, "Laterally driven polysilicon resonant microstructures," *Sens. Actuators*, vol. 20, no. 1/2, pp. 25–32, Nov. 1989.
[32] O. Manzardo, H. P. Herzig, C. R. Marxer, and N. F. de Rooij, "Miniaturized time-scanning Fourier transform spectrometer based on silicon technology," *Opt. Lett.*, vol. 24, no. 23, pp. 1705–1707, Dec. 1999.
[33] W. Noell, P.-A. Clerc, L. Dellmann, B. Guldimann, H.-P. Herzig, O. Manzardo, C. R. Marxer, K. J. Weible, R. Dändliker, and N. de Rooij, "Applications of SOI-based optical MEMS," *IEEE J. Sel. Topics Quantum Electron.*, vol. 8, no. 1, pp. 148–154, Jan./Feb. 2002.
[34] T. Zhao and Y. C. Liang, "New actuation method for push–pull electrostatic MEMS comb drive," *IEEE Trans. Ind. Electron.*, vol. 50, no. 6, pp. 1337–1339, Dec. 2003.
[35] C. Yamahata, D. Collard, B. Legrand, T. Takekawa, M. Kumemura, G. Hashiguchi, and H. Fujita, "Silicon nanotweezers with subnanometer resolution for the micromanipulation of biomolecules," *J. Microelectromech. Syst.*, vol. 17, no. 3, pp. 623–631, Jun. 2008.
[36] S. Timoshenko, *Vibration Problems in Engineering,* 2nd ed. New York: Van Nostrand, 1937, ch. 2.
[37] D. W. Jordan and P. Smith, *Nonlinear Ordinary Differential Equations: An Introduction for Scientists and Engineers,* 4th ed. New York: Oxford Univ. Press, 2007, ser. Oxford Applied and Engineering Mathematics, ch. 7.
[38] M. Stranczl, "Frictionless electrostatic rotary stepper micromotor for microrobotic applications," M.S. thesis, École Polytechnique Fédérale de Lausanne (EPFL), Lausanne, Switzerland, 2011.
[39] M. Stranczl, E. Sarajlic, H. Fujita, M. A. M. Gijs, and C. Yamahata, "High-angular-range electrostatic rotary stepper micromotors fabricated with SOI technology," *J. Microelectromech. Syst.*, vol. 21, no. 3, pp. 605–620, Jun. 2012.
[40] K. L. Turner, S. A. Miller, P. G. Hartwell, N. C. MacDonald, S. H. Strogatz, and S. G. Adams, "Five parametric resonances in a microelectromechanical system," *Nature*, vol. 396, no. 6707, pp. 149–152, Nov. 1998.
[41] I. Kozinsky, H. W. C. Postma, I. Bargatin, and M. L. Roukes, "Tuning nonlinearity, dynamic range, frequency of nanomechanical resonators," *Appl. Phys. Lett.*, vol. 88, no. 25, p. 253 101, Jun. 2006.
[42] M. Agarwal, S. A. Chandorkar, H. Mehta, R. N. Candler, B. Kim, M. A. Hopcroft, R. Melamud, C. M. Jha, G. Bahl, G. Yama, T. W. Kenny, and B. Murmann, "A study of electrostatic force nonlinearities in resonant microstructures," *Appl. Phys. Lett.*, vol. 92, no. 10, p. 104 106, Mar. 2008.
[43] L. C. Shao, C. L. Wong, and M. Palaniapan, "Study of the nonlinearities in micromechanical clamped–clamped beam resonators using stroboscopic SEM," *J. Micromech. Microeng.*, vol. 18, no. 8, p. 085019, Aug. 2008.
[44] F. M. Alsaleem, M. I. Younis, and H. M. Ouakad, "On the nonlinear resonances and dynamic pull-in of electrostatically actuated resonators," *J. Micromech. Microeng.*, vol. 19, no. 4, p. 045013, Apr. 2009.

Christophe Yamahata received the M.Sc. and Ph.D. degrees in microengineering and microsystems from the École Polytechnique Fédérale de Lausanne (EPFL), Lausanne, Switzerland, in 2000 and 2005, respectively.

From 2005 to 2008, he was with the Institute of Industrial Science, The University of Tokyo, Tokyo, Japan. There, he pursued research on biomicroelectromechanical systems as a Postdoctoral Fellow of the Swiss National Science Foundation and, subsequently, as a Japan Society for the Promotion of Science Postdoctoral Fellow. Since December 2008, he has been a Research Associate with the Laboratory of Microsystems, Institute of Microengineering, EPFL. His current research interests are in silicon microsystems for biophysical instrumentation at the molecular and cellular scales.

Marc Stranczl was born in Geneva, Switzerland, in 1986. He received the M.Sc. degree in microengineering from the École Polytechnique Fédérale de Lausanne (EPFL), Lausanne, Switzerland, in 2011.

In September 2009, he joined the Laboratory of Microsystems, Institute of Microengineering, EPFL, as an M.Sc. student, where he completed a semester project and, in the following year, his M.Sc. project on the topic of frictionless electrostatic rotary stepper micromotors. From March to September 2011, he was a Research Assistant with the Institute of Microengineering, EPFL. Since October 2011, he has been a Research Engineer at Nivarox-FAR S.A., Le Locle, Switzerland.

Mr. Stranczl was the recipient of the 2011 Omega Student Prize for his M.Sc. thesis entitled "Frictionless electrostatic rotary stepper micromotor for microrobotic applications."

Edin Sarajlic received the M.Sc. degree in mechanical engineering and the Ph.D. degree in electrical engineering from the University of Twente, Enschede, The Netherlands, in 2001 and 2005, respectively.

From 2005 to 2008, he was a Research Fellow with the Center for International Research on Micromechatronics, Institute of Industrial Science, The University of Tokyo, Tokyo, Japan. He is currently a MEMS Research Engineer with SmartTip B.V., Enschede. His research interest focuses on MEMS, particularly on the development of microactuators and micromachining methods for their fabrication.

Gijs J. M. Krijnen (M'90) received the M.Sc. degree in electrical engineering and the Ph.D. degree from the University of Twente, Enschede, The Netherlands, in 1987 and 1992, respectively.

From 1992 to 1995, he was a Fellow of the Royal Netherlands Academy of Arts and Sciences and studied second- and third-order nonlinear integrated optic devices. During this period, he was a Visiting Scientist at the Center for Research and Education in Optics and Lasers, University of Central Florida, Orlando. From 1995 to 1997, he worked on integrated optic devices for optical telecommunication simultaneously with the University of Twente and Delft University of Technology, Delft, The Netherlands. Since 1998, he has been an Associate Professor in the Transducers Science and Technology Group, MESA+, University of Twente, where he is responsible for microactuator research and, since May 2007, has been the Chair of MEMS Design in the Electrical Engineering Department. His current interests are in lifelike MEMS in general and biomimetic flow sensors in particular.

Martin A. M. Gijs received the B.Sc. and Ph.D. degrees in physics from the Katholieke Universiteit Leuven, Leuven, Belgium, in 1981 and 1986, respectively.

In 1987, he joined Philips Research Laboratories, Eindhoven, The Netherlands. He has worked there on the microfabrication and nanofabrication processes of high-critical-temperature superconducting Josephson and tunnel junctions, the microfabrication of microstructures in magnetic multilayers showing the giant magnetoresistance effect, the design and realization of miniaturized motors for hard-disk applications, and the design and realization of planar transformers for miniaturized power applications. Since 1997, he has been with the École Polytechnique Fédérale de Lausanne, Lausanne, Switzerland, where he is currently a Professor in the Institute of Microengineering and is responsible for the Microsystem Technology Group. His main interests are in developing technologies for novel magnetic devices, new microfabrication technologies for microsystem fabrication in general, and the development and use of microsystem technologies for microfluidic and biomedical applications in particular.